The adjoint method for automotive optimisation using Sphericity based morpher

Christos Kapellos[1], Pavlos Alexias[2] Eugene De Villiers[3]

[1]Volkswagen AG, Group Research, CAE Methods, Wolfsburg, Germany
[2]Engys Srl., Trieste, Italy
[3]Engys Ltd., London, United Kingdom

Summary:

A robust workflow for shape optimisation of internal and external flows with application to automotive design is demonstrated in this paper. A gradient based approach is presented, in which the surface sensitivity with respect to the flow variables is computed with the continuous adjoint method. For aerodynamic shape optimisation cases, mesh displacement algorithms are indispensable in order to avoid re-meshing the updated geometry in each optimisation step. Keeping the same mesh topology at every optimisation cycle secures gradient consistency and the possibility to use the previous solution as initial conditions in order to converge the CFD equations faster. Simple mesh displacement algorithms, such as the spring analogy, run into problems under complex surface deformations. Thus a mesh optimisation approach can be proved to be more robust as it copes better with complex elements optimising also the base mesh. In this paper the mesh displacement algorithm is based on sphericity, which quantifies the mesh quality. Solving an extra optimisation problem for the maximisation of the sphericity value, results in the new internal mesh nodes positions. The methodology is heuristic in nature in that it does not consider known numerical quality metrics explicitly. It has shown however to be exceptionally robust and effective allowing the maintenance of high cell quality even during extreme deformation events. The suggested method is applied to automotive test cases of internal and external aerodynamics. In such cases, the use of a robust morpher which preserves geometry features and delays mesh quality deterioration is found to be crucial.

1 Introduction

Optimisation methods have emerged through the years to an essential element for automotive aerodynamic design. Stochastic methods, such as evolutionary algorithms, are already established in industry due to their highly explorative character and modular ability, with the drawback however of many evaluations of the cost function. Gradient-based methods, on the other hand, can reduce significantly the computational cost and offer more control in handling constraints and preserving design features which should not change drastically during the optimisation.

The adjoint method, in particular, computes the gradient of the desired objective function with respect to (w.r.t.) the design variables with a computational cost practically independent of the number of design variables and comparable to that of solving the primal equations, for aerodynamics the Navier Stokes equations [1]. To this end, the adjoint equations, their boundary conditions and the final expression of the gradient, namely the sensitivity derivative, are derived by differentiating the objective function augmented by the volume integrals of the primal equations multiplied by the adjoint variables. The adjoint equations are then discretised similarly to the primal equations and solved in order to compute the objective function gradient.

In adjoint shape optimisation either a parametrised description of the shape or the surface nodes of the mesh are used as design variables. In the latter approach, the design space is obviously the richest possible for the current spatial discretisation of the shape. However, any noise introduction in the adjoint derivatives combined with the fact that each surface node is being perturbed independently from its neighbours can create oscillations and irregularities. This will reduce the smoothness of the deformed shape which can make the optimisation problem difficult to converge or even diverge. It is thus necessary to create a smooth representation of the gradient in order to cut-off any unnecessary oscillations. In the literature there are various methods on the proper smoothing of the sensitivity derivatives. The most well-established are an explicit technique which uses convolution filter kernels [2] and an implicit smoothing technique [3], also called Sobolev gradient.

Furthermore, a mesh displacement algorithm is indispensable in order to deform the volume mesh according to the movement of the surface boundary without being necessary to re-mesh the new geometry. The mesh topology in this case will remain the same securing gradient consistency through the optimisation cycles. Many mesh displacement algorithms have been developed so far following a variety of approaches, like elastic medium analogy [4], spring analogy [5] and Radial Basis Functions [6] methods. In our study the mesh displacement algorithm is based on a mesh quality metric called sphericity [7]. Solving the optimisation problem for the maximisation of the sphericity value, results in the new positions of the points inside the mesh.

In this paper a workflow for shape optimisation in internal and external aerodynamics is demonstrated. The objective function gradient is computed with the continuous adjoint method, as formulated in section 2. The sensitivity derivatives are afterwards smoothed using the implicit technique and used to move the boundary and internal mesh, which is then optimised based on its sphericity, as described in section 3. The method is implemented in OPENFOAM. The flow solver is the standard steady state incompressible solver, while the adjoint solver is provided by Engys [8]. The proposed workflow is applied to two industrial cases, targeting at power dissipation minimisation of an automotive air duct and at drag reduction of the DrivAer car model [9], developed by the Institute of Aerodynamics and Fluid Mechanics of Technical University Munich (TUM).

2 The continuous adjoint method

In this section a brief description of the continuous adjoint method for the incompressible Navier-Stokes equations [10] is presented. A general objected function is defined on the boundary, so as to accommodate for both internal and external flow cost functions which are investigated later.

2.1 Flow Equations

The flow is modelled by the Navier-Stokes equations for incompressible flows that read

$$R^p = \frac{\partial v_i}{\partial x_i} = 0$$

$$R_i^v = v_j \frac{\partial v_i}{\partial x_j} - \frac{\partial \tau_{ij}}{\partial x_j} + \frac{\partial p}{\partial x_i} = 0, \qquad i = 1,2,3$$

where p is the static pressure, v_i is the flow velocity, $\tau^{ij} = (\nu + \nu_\tau)\left(\frac{\partial v_i}{\partial x_j} + \frac{\partial v_j}{\partial x_i}\right)$ are the components of the stress tensor and ν and ν_τ the kinematic and turbulent viscosity respectively. The turbulence model used is the Spalart-Allmaras turbulence model described by

$$R_i^{\tilde{\nu}} = v_j \frac{\partial \tilde{\nu}}{\partial x_j} - \frac{\partial}{\partial x_j}\left[\left(\nu + \frac{\tilde{\nu}}{\sigma}\right)\frac{\partial \tilde{\nu}}{\partial x_j}\right] - \frac{c_{b2}}{\sigma}\left(\frac{\partial \tilde{\nu}}{\partial x_j}\right)^2 - \tilde{\nu}P + \tilde{\nu}D = 0$$

where $\tilde{\nu}$ is the model variable [11].

2.2 Objective functions

Two different objective functions are investigated. In the internal flow test case, power dissipation [12] is the cost function to be minimised, while in external aerodynamics it is the drag force [13]. These read respectively

$$F_{power} = \int_S \left(p + \frac{1}{2} v_i^2\right) v_i \, n_i dS$$

and

$$F_{drag} = \int_S \left(p\delta_j^i - \tau_{ij}\right) n_j r_i dS$$

In what follows a generalised expression of an objective function defined on the boundary will be used, given by

$$F = \int_S F_s \, n_i dS$$

2.3 The continuous adjoint formulation

The objective function is firstly augmented with the field integrals of the flow equations multiplied with the adjoint variables.

$$J = F + \int_\Omega u_i R_i^v \; d\Omega + \int_\Omega q R^p \; d\Omega$$

Here, u_i and q are the adjoint to the flow velocity and static pressure respectively. Although the turbulent equation can also be included in the augmented function, by introducing an extra adjoint variable and raising so the “frozen turbulence” assumption, it was not deemed necessary in the scope of this paper. Next step is the differentiation of the augmented cost function and the application of the Green-Gauss theorem where necessary. Finally, by zeroing the multipliers of the partial derivatives of flow variables, the field adjoint equations, boundary conditions and the expression of the sensitivity derivatives are obtained.

The adjoint equations yield

$$R^q = \frac{\partial u_i}{\partial x_i} = 0$$

$$R_i^u = u_j \frac{\partial v_j}{\partial x_i} - \frac{\partial (v_j u_i)}{\partial x_j} - \frac{\partial \tau_{ij}^a}{\partial x_j} + \frac{\partial q}{\partial x_i} = 0, \qquad i = 1,2,3$$

where $\tau_{ij}^a = (\nu + \nu_\tau)\left(\frac{\partial u_i}{\partial x_j} + \frac{\partial u_j}{\partial x_i}\right)$ are the components of the adjoint stress tensor.

The expression of the sensitivity derivatives w.r.t. the design variables b_n is given by

$$\frac{\delta J}{\delta b_n} = -\int_S \left(u_i v_j n_j + \tau_{ij}^a n_j - q n_i + \frac{\partial F_j}{\partial v_i} n_j\right) \frac{\partial v_i}{\partial x_k} n_k \frac{\delta x_m}{\delta b_n} n_m dS$$

3 Implicit smoothing, mesh deformation and mesh optimisation

In this section the procedure with which the computed sensitivity derivatives are smoothed and used to move the surface mesh and the volume mesh is described. The process comprises three steps, the gradient implicit smoothing, the mesh deformation and the mesh optimisation.

3.1 Gradient Implicit Smoothing

The computed sensitivity derivatives are smoothed with the implicit method, where the new smoothed sensitivities $\bar{G}$ are being calculated solving the equation

$$\bar{G} - \varepsilon \nabla^2 \bar{G} = G$$

where ϵ is the smoothing intensity. The smoothing intensity ϵ is a case dependent parameter and depends mostly on the oscillations amplitude w.r.t. the surface area of the boundary faces.

.

3.2 Mesh Deformation and optimisation

The computed displacement on the surface to be optimised is then propagated to the interior by solving the Laplacian equation to compute the new coordinates of the internal mesh nodes and the mesh is then optimised relative to its sphericity.

Sphericity is an element wise geometric property which defines how spherical a geometrical object is and is defined as

$$Sph = \frac{\left(\frac{6}{\pi} V_0\right)^{1/3}}{\left(\frac{1}{\pi} S_0\right)^{\frac{1}{2}}}$$

where V_o is the volume and S_o is the surface of the object. In other words, sphericity is the ratio between the diameter of a sphere, that has the same volume with the object, and the diameter of a sphere that has the same surface area as the object (considering that for a sphere holds $S = \pi^{1/3}(6V)^{2/3}$). Given this the sphericity of a sphere is unity by definition and unity is the largest value that any three-dimensional object can have.

There is a variety of methods in the literature using same kind of quality metrics and approaches for mesh optimization and quality improvement. Escobar et al.'s [14] and Kim et al.'s [15,16] are using similar quality metrics introducing the cell perimeter or the RMS cell surface value. The novelty of our method is that the quality metric suggested is appropriate for simultaneous mesh untangling and quality improvement, while additionally an analytical differentiation of the objective function is taking place making the optimization procedure highly accurate and fast.

3.2.1 Mesh Optimisation

Considering for instance a finite volume mesh (structured or unstructured), each cell will have a sphericity value calculated as a function of the cell's surface and volume. This way sphericity will represent the quality level of a cell, in a sense that high sphericity values correspond to good quality cells (highly isotropic) and, on the other hand, low sphericity values are illustrating low quality cells (high skewness, non-orthogonality, etc.).

The goal is to simultaneously maximize each cell's sphericity by re-positioning the vertices of the mesh maintaining however the same mesh topology. To do so, it is necessary to define a point-wise objective function and calculate its derivative w.r.t. the point position. In this way, a gradient based method can be used in order to solve the optimisation problem for the maximization of the point-based objective function.

Assuming that a point P inside the computational mesh is surrounded by M cells we define as an objective function the arithmetic mean of the sphericity values from all the surrounding cells

$$F_p = \frac{1}{M} \sum_{i=1}^{M} Sph_i$$

Differentiating this w.r.t. the point position $\vec{P}$ we get,

$$\overrightarrow{G_p} = \frac{1}{M}\sum_{i=1}^{M}\frac{dSph_i}{d\vec{P}}$$

and the derivative of sphericity w.r.t. $\vec{P}$ is

$$\frac{dSph}{d\vec{P}} = \frac{d\frac{\left(\frac{6}{\pi}V_c\right)^{1/3}}{\left(\frac{1}{\pi}S_c\right)^{1/2}}}{d\vec{P}} = -\frac{3^{\frac{1}{3}}\pi^{\frac{1}{6}}V_c(P)^{\frac{1}{3}}S_c'(P)}{2^{\frac{2}{3}}S_c(P)^{\frac{3}{2}}} + \frac{2^{\frac{1}{3}}\pi^{\frac{1}{6}}V_c'(P)}{3^{\frac{2}{3}}\sqrt{S_c(P)}V_c(P)^{\frac{2}{3}}}$$

where $S_c'(P)$ and $V_c'(P)$ are the derivatives of the cell surface and cell volume w.r.t. the position of the point P respectively. For the analytical differentiation of those geometric values one can refer to [8] to see the full differentiation procedure.

Once the derivatives of all the grid points are calculated, a new set of point positions is obtained by moving each point towards the direction of its derivative. Thus,

$$\overrightarrow{P^{new}} = \vec{P}^{old} + \alpha \cdot \overrightarrow{G_p}$$

where α is the step length of the optimisation cycle. Using a constant value of α is not optimal for the proposed application due to large variations in cell sizes encountered in different CFD meshes. It is therefore necessary to have an adaptive step length. This can be achieved effectively by using second derivatives which also has the added benefit of speeding up the convergence. Based on Nocedal [17] a limited memory BFGS algorithm is constructed for building and updating the inverse Hessian matrix of the second derivatives. Thus, the latter equation can be written as

$$\overrightarrow{P^{new}} = \vec{P}^{old} + \lambda H_p^{-1} \cdot \overrightarrow{G_p}$$

where H_p^{-1} is the inverse Hessian matrix and λ is a step length which will guarantee that moving towards the direction $H_p^{-1}\overrightarrow{G_p}$ an improvement in the objective function will be achieved (Wolfe conditions [18]).

4 Application of the workflow

4.1 Internal flow: automotive air duct

A segment of an automotive air duct is optimised here targeting at power dissipation minimisation. The flow is laminar with a Reynolds number of 350 and the mesh is structured comprising 700000 cells. During the optimisation only the S-Bend portion of the duct is allowed to be modified. To achieve an even smoother transition of the sensitivities values, a sigmoid filter was used at the boundary between the deformable and constrained patches.

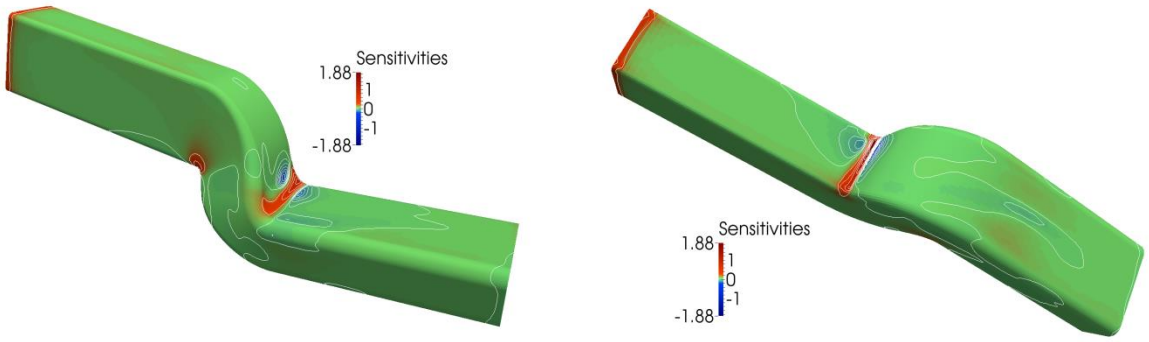

Fig. 1: Sensitivity map calculated for the starting geometry of the S-Bend case targeting at minimising power dissipation. Red areas have to be pulled away from the fluid, while blue areas have to be pushed towards it, in order to minimise the objective function.

As seen in fig. 1. the sensitivities computed at the first optimisation cycle, expectedly tend to 'straighten up' the S-Bend, so that the recirculation area is supressed. After the completion of 40 optimisation cycles the power dissipation was reduced by 17.1%. The optimised shape and mesh have preserved their smoothness and quality respectively (fig. 2). It is also interesting to notice, that although in many cycles after the boundary movement and the internal nodes displacement the mesh quality deteriorated, comprising many skewed and non-orthogonal elements, the mesh optimisation managed always to improve the quality of each and every bad element (fig.3).

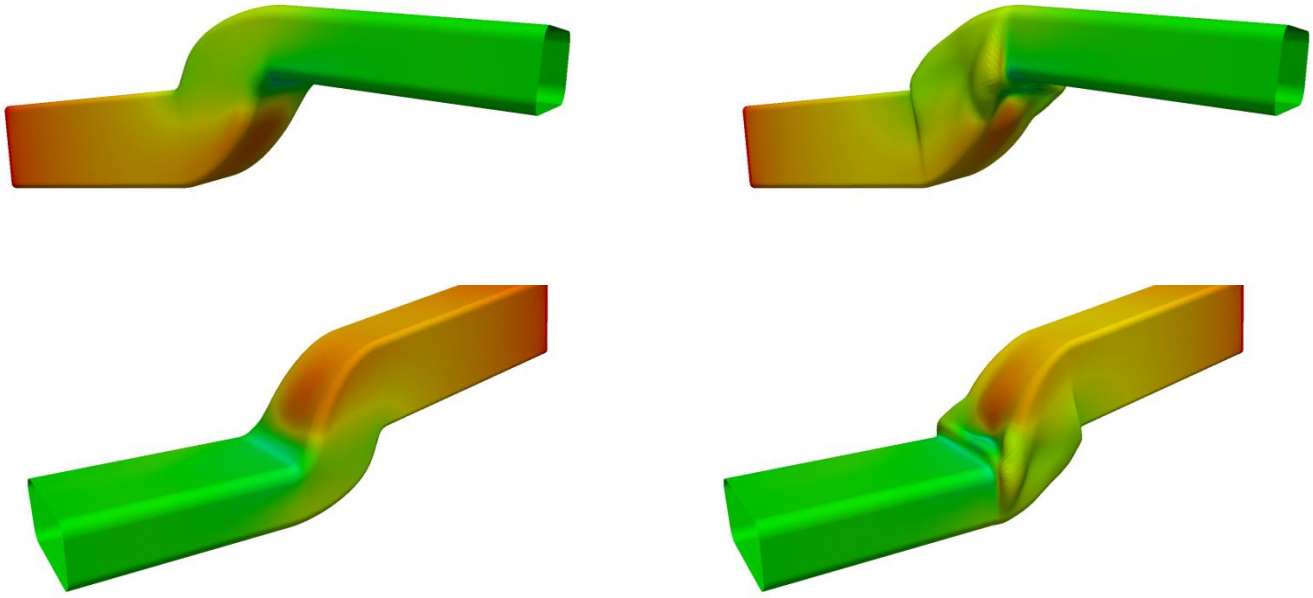

Fig. 2: Starting (left) and optimised (right) geometry of the S-Bend. The optimised geometry was obtained after 40 optimisation cycles leading to a 17.1% reduction in the objective function. The geometries are coloured with the pressure distribution.

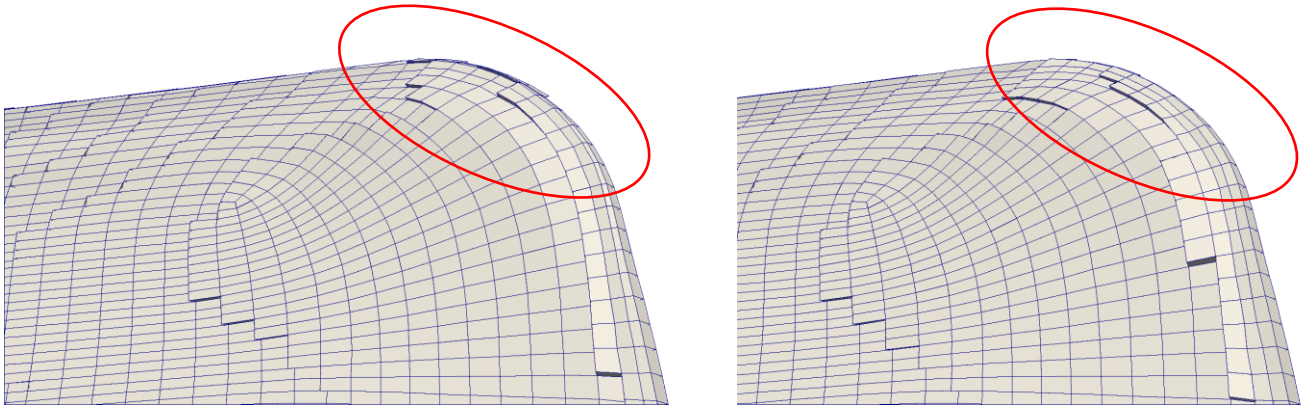

Fig. 3: Slice of the internal mesh before (left) and after (right) the mesh optimisation. In the area denoted on the red circle there are highly non-orthogonal faces as well as some collapsed cells. After the mesh optimisation the mesh quality is highly improved.

4.2 External aerodynamics: DrivAer vehicle

In this section, the optimisation workflow is applied to the DrivAer car model aiming at drag minimisation. The fast-back configuration with a smooth underbody, with mirrors and wheels (FS wm ww) is used (Fig. 4). The flow is turbulent and modelled with the Spalart-Allmaras turbulence model. The half car is meshed and simulated with a computational grid comprising around 7 million cells. Only the rear part of the car is allowed to deform, since its shape is critical to the flow in the wake of the car and hence to its drag.

In Fig. 5 the sensitivity derivatives on the DrivAer car model computed at the first optimisation cycle are presented. Focusing on the rear part of the car, the sensitivity map suggests the creation of a spoiler, by lowering the area just before the edge where the flow separates. Furthermore, on the rear fender an area appears which has to be pulled towards the fluid. For the smoothing procedure, the variable in the implicit equation was selected so that a larger area is affected. Since the rear part is moved in a more rigid way the creation of new “feature” lines is avoided.

After the completion of 10 optimisation cycles the total drag of the optimised geometry is reduced by around 0.7%. The area with the highest deformation is located in the end of the trunk, which is pushed inwards and creates a spoiler (fig. 6). This total drag reduction may seem small, but is significant, considering that only a small portion of the rear part surface is displaced.

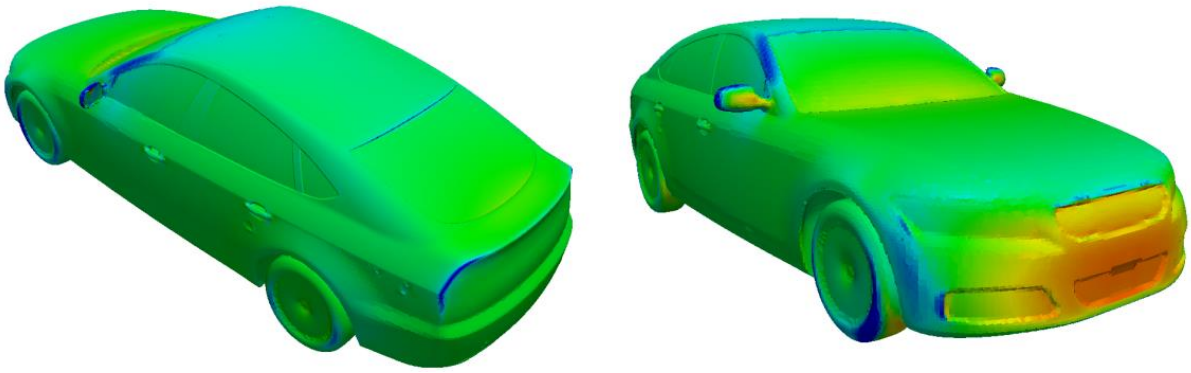

Fig. 4: Pressure distribution on the starting geometry of the DrivAer car model, fast-back, smooth underbody, with mirrors, with windows (FS wm ww).

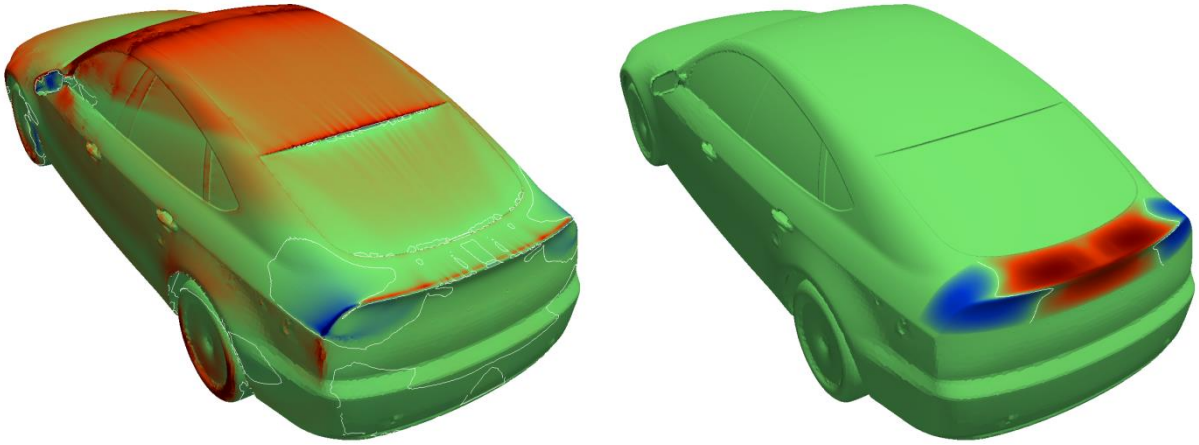

Fig. 5: Raw (left) and smoothed (right) sensitivity map targeting at drag minimisation computed at the first optimisation cycle. Red areas have to be pulled away from the fluid, while blue ones towards it, in order to reduce drag force. Iso-lines denote zero sensitivity areas.

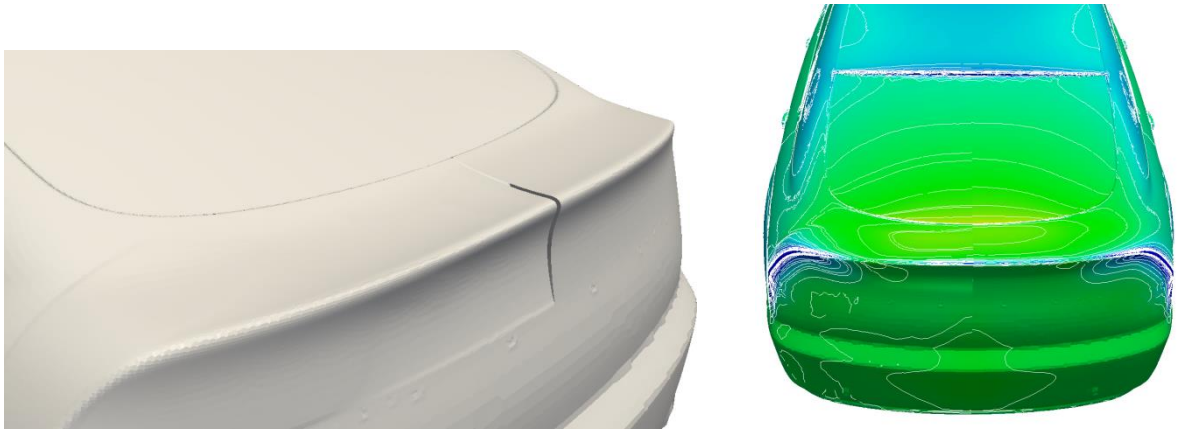

Fig. 6: Comparison between the optimised (left half of the car) and starting (right half) rear part geometries of the DrivAer model. On the right the pressure distribution for both the optimised and starting geometry is presented.

5 Conclusions

In this paper a workflow for aerodynamic shape optimisation was presented and applied to several testcases. For the gradient-based optimisation algorithm the objective function gradient is computed with the continuous adjoint method. The sensitivity derivatives are smoothed with an implicit technique and the boundary and internal mesh nodes are moved accordingly. In the final step the mesh quality is improved through an optimisation routine which aims at the maximisation of element sphericity, a mesh quality metric. The workflow was applied to two industrial cases of internal and external aerodynamics. In both cases the objective function value was reduced significantly proving the presented approach to be robust and efficient.

6 Acknowledgements

This work has been conducted within the IODA project (http://ioda.sems.qmul.ac.uk), funded by the European Union HORIZON 2020 Framework Programme for Research and Innovation under Grant Agreement No. 642959.

7 References

[1] Nadarajah, S., Jameson, A.: “Studies of the continuous and discrete adjoint approaches to viscous automatic aerodynamic shape optimization”, AIAA Paper, 2001, 25(30)

[2] Stuck, A. and Rung, T.: “Filtered Gradients for Adjoint-based Shape Optimisation”, 20th AIAA Computational Fluid Dynamics Conference 27 - 30 June 2011, Honolulu, Hawaii
[3] Jameson, A. and Vassberg, J.C.: “Studies of alternative numerical optimization methods applied to the brachistochrone problem”, Computational Fluid Dynamics, 2000, 9:281-296
[4] Amirante, D. and Hills, N.J. and Barnes, C.J.:“A moving mesh algorithm for aero-thermomechanical modelling in turbomachinery”, International Journal for Numerical Methods in Fluids, 2012, vol. 70, 1118–1138
[5] Batina, J.: ”Unsteady Euler algorithms with unstructured dynamic mesh for complex-aircraft aerodynamic analysis”, AIAA Journal, 29(3):327-333
[6] Sieger, D., Menzel, S. and Botsch, M.: ”RBF Morphing Techniques for Simulation-based Design Optimization”, Engineering with Computers, 2014, 30(2):161174
[7] Alexias P., De Villiers E. "Sphericity: Mesh optimization for arbitrary element topology”, VII ECCOMAS Congress, 5-10 June 2016, Crete Island, Greece
[8] Georgios K. Karpouzas, Evangelos M. Papoutsis-Kiachagias, Thomas Schumacher, Eugene de Villiers, Kyriakos C. Giannakoglou, Carsten Othmer: “Adjoint Optimization for Vehicle External Aerodynamics”, International Journal of Automotive Engineering, 2016, Vol.7,No.1,pp.1-7
[9] Heft, A., Indinger, T., Adams, N.: “Experimental and numerical investigation of the DrivAer Model”, ASME 2012, Symposium on Issues and Perspectives in Automotive Flows, pp. 41–51. Puerto Rico, USA
[10] Papoutsis-Kiachagias, E., Giannakoglou, K.: “Continuous adjoint methods for turbulent flows, applied to shape and topology optimization: Industrial applications”, Archives of Computational Methods in Engineering, 2014, 10.1007/s11831-014-9141-9
[11] Spalart, P., Jou, W., Stretlets, M., Allmaras, S.: “Comments on the feasibility of LES for wings and on the hybrid RANS/LES approach”, Proceedings of the first AFOSR International Conference on DNS/LES, 1997
[12] Othmer, C.: “A continuous adjoint formulation for the computation of topological and surface sensitivities of ducted flows”, International Journal for numerical methods in fluids, 2008, 58:861-877
[13] Othmer, C.: “Adjoint methods for car aerodynamics”, Journal of Mathematics in Industry, 2014, 4:6
[14] J.M. Escobar, E. Rodríguez, R. Montenegro, G. Montero, J.M. González-Yuste, Simultaneous untangling and smoothing of tetrahedral meshes, Computer Methods in Applied Mechanics and Engineering, Volume 192, Issue 25, 20 June 2003, Pages 2775-2787, ISSN 0045-7825
[15] Jibum Kim, “An Efficient Approach for Solving Mesh Optimization Problems Using Newton’s Method,” Mathematical Problems in Engineering, vol. 2014, Article ID 273732, 9 pages, 2014. doi:10.1155/2014/273732
[16] Kim, J., Panitanarak, T. and Shontz, S. M. (2013), A multiobjective mesh optimization framework for mesh quality improvement and mesh untangling. Int. J. Numer. Meth. Engng, 94: 20–42. doi:10.1002/nme.4431
[17] Nocedal, J.:”Updating Quasi-Newton Matrices with Limited Storage”, Mathematics of Computation, 1980, Vol. 35, No. 151, pp. 773-782.
[18] Wolfe, P.:”Convergence Conditions for Ascent Methods”, SIAM Review 11 (2): 226000